AD-A247 663

DTIC
ELECTE
MAR 18 1992
S D
D

Final Technical Report

Seafloor Pressure Array Studies at Ultra-Low Frequencies

John A. Orcutt
Principal Investigator

Office of Naval Research Grant
N00014-90-J-1228

This document has been approved for public release and sale; its distribution is unlimited.

California Univ. San Diego
La Jolla

Statement A per telecon Dr. Marshall Orr
ONR/Code 1125
Arlington, VA 22217-5000

NWW 3/17/92

per telecon ONR 3/20/92 cl

92-04803

Abstract

Broadband inertial measurements of environmental noise on the seafloor have always been difficult technically and few examples of successful measurements are available. A knowledge of environmental noise processes, however, is essential for future broadband instrument design and deployment. In order to measure broadband noise routinely, a low frequency pressure gauge designed for deep ocean recording was adapted for use with the Scripps' OBSs and calibrated in the laboratory. The instruments were deployed twice in array configurations along with other pressure sensors in 4.1-km deep ocean southwest of San Diego, California. Spectra from the hydrophones showed a stable 0.15 Hz microseism peak throughout the deployment period with some evidence of dispersion. Smaller peaks at 0.3-1 Hz appeared when the local wind became stronger. Highly coherent peaks at 0.085 Hz, originally interpreted as 'single frequency microseisms', were found to be Rayleigh wavetrains from large earthquakes. Reverberations in the water column caused by P-wave arrivals from the earthquakes were also observed. Coherence in the microseism band was significant only for instruments separated by less than 6 km, lending support to the hypothesis that the source is at least in part isotropic and random. Wavenumber analysis was successful only for the well-defined earthquake signals while for the microseism band, low coherence and the location of the sensors reduced the array's useful azimuthal resolution.

Introduction

Long period seismic recordings on and below the Earth's surface have invariably shown the presence of background signals (see Orcutt et al, 1992, for a review). In the low frequency band, between 0.01 and 1 Hz, the most prominent feature is the microseism peak, at 0.1-0.2 Hz, which has been a familiar feature reported in seismological records for almost a century. Microseism signals were found to be closely related to oceanic storms and their amplitude was shown to be dependent on coastal wave amplitude. Darbyshire (1950) found a two-to-one relation between the periods of the waves and the microseism peak which was explained by the theory of the origin of microseisms developed by Longuet-Higgins (1950). The theory discusses the nonlinear interaction between two waves of the same frequency and of similar, but opposing wavenumber. Waves traveling on the surface of the ocean in opposite directions will produce pressure variations at twice their frequency and an amplitude that is proportional to the product of both amplitudes. These signals do not attenuate with depth and will, therefore, be felt on the deep ocean floor with double the frequency of the wind waves. It was suggested that incoming and reflected coastal waves can interact to produce microseisms close to the coast. This was confirmed by data from stations along the coast where a peak at about 0.085 Hz was recorded. This frequency agreed with the dominant ocean wave frequency which was half the frequency of the microseism peak (Haubrich et al, 1963). This lower frequency feature was named the 'single frequency peak' and was recognized as a source of the microseism peak, termed

accordingly, the 'double frequency peak'.

In the past thirty years, the field of microseism studies had advanced with the development of Ocean Bottom Seismometers (OBSs). Seismometers and hydrophones were placed on the sea bed (Latham et al, 1967 ; Nichols, 1981; Kibblewhite and Ewans, 1985) and background signal levels below 1 Hz were found to be comparable or higher than those of land recordings. The studies reported that the microseism spectral peaks between 0.1 and 0.35 Hz were associated with elastic waves which propagated primarily as Rayleigh waves. The microseism levels were related to weather systems and incoming and reflected coastal waves. Until recently, most of the ocean bottom data were acquired from single instrument deployments combined with surface or land based recordings. These confirmed the Rayleigh wave properties of the signals and showed that the weather systems, wave action and microseism activity are directly related. Although the non-linear interaction of opposing waves was recognized as the source mechanism for generating microseisms, several systems were suggested as possible sources for signals recorded in the deep ocean. Webb and Cox (1984) found that incoming swell and waves reflected from the shoreline can interact to produce microseisms at distances of over 1000 km from the coast. Storms in the ocean generate waves which travel in opposite directions (Tyler, 1977) and a change in the wind direction can also create waves traveling in opposing directions. In order to establish a direct link between microseism signals and their source it was necessary to record data in the spatial domain which would provide information on the direction from which the signal was arriving. The experiments described in this paper were aimed at studying the propagation characteristics of the microseisms by placing arrays of sensors on the ocean bottom and recording the background signals over a period of a few weeks. Hydrophones which were sensitive at low frequencies and were capable of long term deployment were used for the first time with the Scripps' OBSs. The calibration tests for the instruments are described at the beginning of this paper followed by a description of the experiment for recording ambient signals in deep water and its results.

Instrumentation

Low frequency signals in the microseism band are related to weather and wave phenomena which change over periods of days and weeks. It was, therefore, essential to use instruments which were capable of long-term deployment and considerable data storage capacity. Another feature necessary for a study of this nature is instrument sensitivity extending well below the microseism band. OBSs have been used by Scripps repeatedly for long-term (over one month) deployments in the deep ocean, but their response, particularly that of the hydrophone channel, falls off rapidly below the microseism band (Moore et al, 1981). A differential pressure gauge, developed for low frequency recordings by Cox et al (1984) and sensitive to frequencies below 10 mHz was chosen to replace the conventional OBS hydrophone with only slight modification to the OBS electronics. We present here a brief description of the OBS; for a detailed description of the hardware and software see Moore et al (1981) and Orcutt et al (1987). The seismometers are Mark Products L-4-3D geophones, with a voltage output proportional to velocity and a natural frequency of 1 Hz. The pressure sensor is the Cox-design differential pressure gauge (Cox et al, 1984) with a sensitivity

range of 0.01-5 Hz. The high sensitivity of the pressure gauge is achieved by measuring differential rather than absolute pressure. The gauge measures the difference between outside pressure fluctuations passing through a diaphragm and a reference chamber which is pressurized to the average ambient pressure. A block

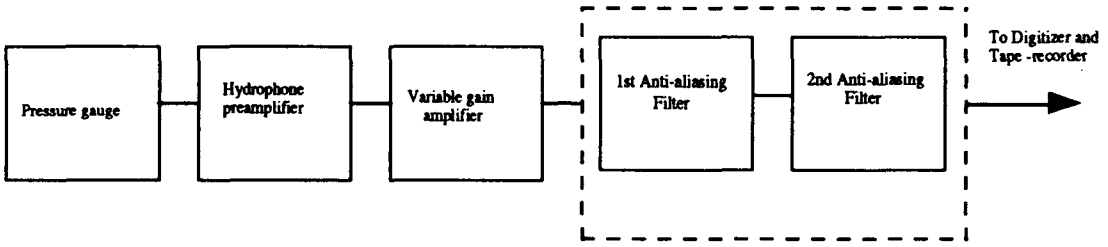

Figure 1: Block diagram of the OBS hydrophone channel

diagram for the new OBS hydrophone channel is shown in figure 1. The sensor outputs are passed through a preamplifier, a variable gain amplifier which is digitally controlled to adjust for varying Earth noise levels, and anti-aliasing filters before quantization by a 12-bit analog-to-digital converter. The data are finally recorded on magnetic tape in a serial format. The recording scheme for these experiments was set prior to launch and 25 hours of recording time were available at a 32 sample-per-second rate. The OBS is released from the anchor for recovery either by acoustic release or preset timers.

Calibrating the new hydrophone

The new hydrophones were designed and built at the Scripps Institution of Oceanography (Cox et al, 1984) for deep-ocean recordings of low-frequency signals. Theoretical output values were used for designing the OBS circuit changes, but it was necessary to calibrate them empirically to produce the instrument response required for quantitative measurements. A simple method was devised to create a calibrated pressure signal from which the hydrophone's impulse response could be inferred.

The hydrophone was placed inside a standard bell jar and the air was pumped out using a vacuum pump (see figure 2). By opening a release valve, air was let back into the chamber, thereby creating the calibration signal. A pressure sensor, identical to the one inside the hydrophone, was placed inside the pressure chamber and recorded the input signal. The hydrophone connector cable was connected to the preamplifier which was placed outside the chamber. Power was supplied by a DC power supply which provided ±12 V to the preamplifier. The output signal was recorded on a Nicolet digital oscilloscope and saved on floppy disk.

Since a 'random pressure signal' (analogous to random telegraph signal) is somewhat difficult to generate in the laboratory, another calibrating signal that contained all frequencies had to be used. An ideal signal would be an impulse or delta function, but a pressure impulse signal is, of course, impossible to create. We chose, therefore, to use a step function and by either dividing the output response by the input response in the frequency domain, or taking the derivative of the output in the time domain, the response of the system to a range of frequencies could be measured.

Dist | Special
A-1

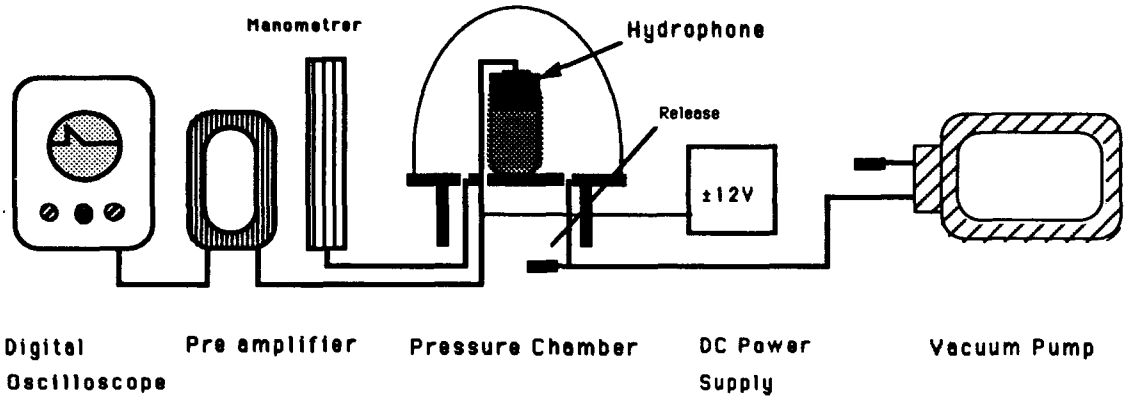

Figure 2: The calibration experiment setup

To generate the calibration signal, air was pumped out of the bell jar to a vacuum of 1 inch Hg or $3.39 \cdot 10^3$ Pa. After the pressure gauge reached equilibrium, the release valve was opened, letting the air in thereby producing a step function in air pressure. The step function and output signal were recorded simultaneously on the digital oscilloscope. A typical output signal is plotted in figure 3. The long term response decays because of the capillary leak, which allows flow between the ambient and reference chambers thereby relaxing the induced pressure. The average decay time for the response is 100 seconds.

The transfer function could intuitively be calculated by dividing the frequency transform of the output signal by the frequency transform of the input signal. Simple spectral division, however, is unstable so the input signal was used only to measure *dp*, the pressure change over the step, for scaling the response in Volts/ Pascal. The transfer function was calculated by taking the derivative of the output response.

The high frequency part of the calibration signal was governed by the time it takes the air to flow through the release valve into the chamber and we found that the signal produced by the air flow did not contain useful frequencies higher than 1 Hz. In order to extend the input signal to higher frequencies, a hydrostatic pressure signal was used. The hydrophone was placed in a water container and allowed to reach equilibrium. It was then lifted abruptly out of the water, thus producing the step pressure change. The transfer function was calculated in the same manner as for the pressure chamber calibration and produced a response

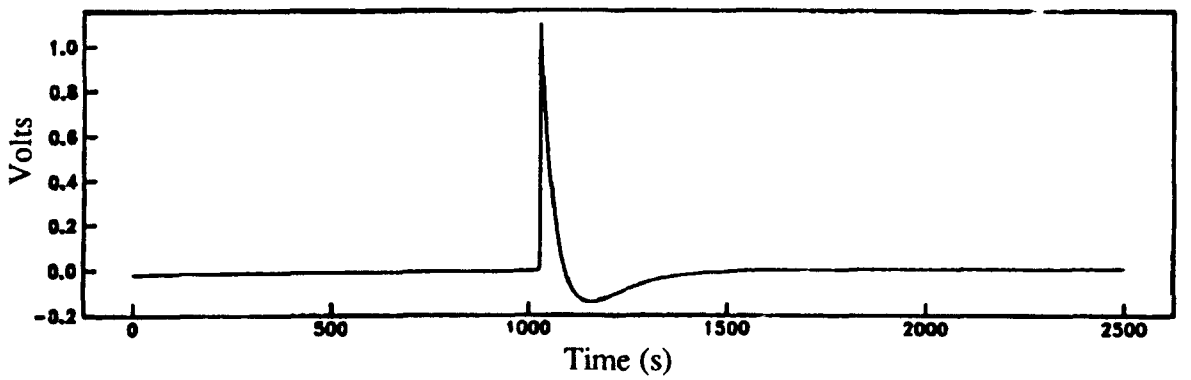

Figure 3: Pressure gauge response to calibration step function.

function which is flat up to 3-4 Hz which is the highest frequency present in the source.

While recording ocean noise data, the OBSs were deployed at a depth of about 4000 meters, where the ambient pressure would be close to 400 Atm and temperatures around 0° C. When designing the hydrophone, Cox et al (1984) addressed the problem of changes in the hydrophone's characteristics due to ambient temperature and pressure. These problems were overcome by insulating the pressure gauge from thermal effects and choosing silicone oil with compressibility and viscosity which are relatively insensitive to pressure and temperature changes. The compressibility and viscosity of 500 cS silicone oil, the one used in the hydrophone, at deep seafloor conditions is unknown. However, assuming its properties are similar to those of 10 cS silicone oil, whose compressibility is known, and that viscosity changes are proportional to compressibility changes, the change in the time constant of the system at ocean bottom temperature and pressure will not be larger than a factor of 2.

A calibration test identical to the one described above was performed at 0°C, and the results confirmed that the calibration was insensitive to temperature. Unfortunately, it was not possible to perform the calibration test under pressure similar to that of the ocean bottom and it is hoped that the changes due to high pressure do not differ much from those due to temperature changes.

The calibrated frequency response can be represented in a compact form as the ratio of two complex polynomials. Berger et al (1979) developed an iterative method for finding these polynomials by least-square fitting their ratio to the given complex response. This method was used on the complex frequency response to approximate the transfer function in terms of poles and zeroes. The initial guess of the number of poles and zeroes was based on the theoretical transfer functions of the pressure gauge and the preamplifier (Lahav, 1991) where only those poles within the frequency range of the calibrated response were taken into account. Because the frequencies achieved in the calibration rig were rather low, the fit was made only at the lower frequencies up to about 0.1 Hz, which means only two out of the five poles in the transfer function were derived directly from the data (the pressure gauge pole and the first pre-amp pole). There were no zeroes and the poles were found to be $(-0.0033)^{-1}$ and $(-0.002)^{-1}$. The three higher frequency poles, which are well known from the preamplifier's electronic component values, were added to the transfer function of the fitted poles to account for behavior at frequencies higher than those produced by the calibration experiment. With a normalizing constant and a second order term in the numerator, the transfer function for the pressure gauge and the preamplifier is

$$H_1(f) = \frac{37.1 \cdot (-f^2)}{(1 + \frac{i \cdot f}{0.0033})(1 + \frac{i \cdot f}{0.002})(1 + \frac{i \cdot f}{31.38})(1 + \frac{i \cdot f}{33.83})(1 + \frac{i \cdot f}{29.38})} \frac{mV}{Pa}$$

The transfer function for the anti-aliasing filter, designed for a 32 Hz sampling rate, is

$$H_2(f) = \frac{-54.41 \cdot i \cdot f}{1 + 19.53 \cdot i \cdot f - 2.78 \cdot f^2 - 0.3706 \cdot f^3} \cdot \frac{-2.8}{1 + 0.142 \cdot i \cdot f - 0.019 \cdot f^2}$$

Figure 4 shows the overall transfer function for the hydrophone channel, $H(f) = H_1(f)H_2(f)$ which was used for filtering the data presented in this paper.

The ocean bottom array experiments

The data described in this paper were collected during two deployments, in May 1986 and May 1988. The experiment sites, shown in figure 5, were chosen for their relatively flat topography and proximity to Scripps' home port of San Diego. The instruments were set on a thin (about 100 m) sediment layer in 4.1-

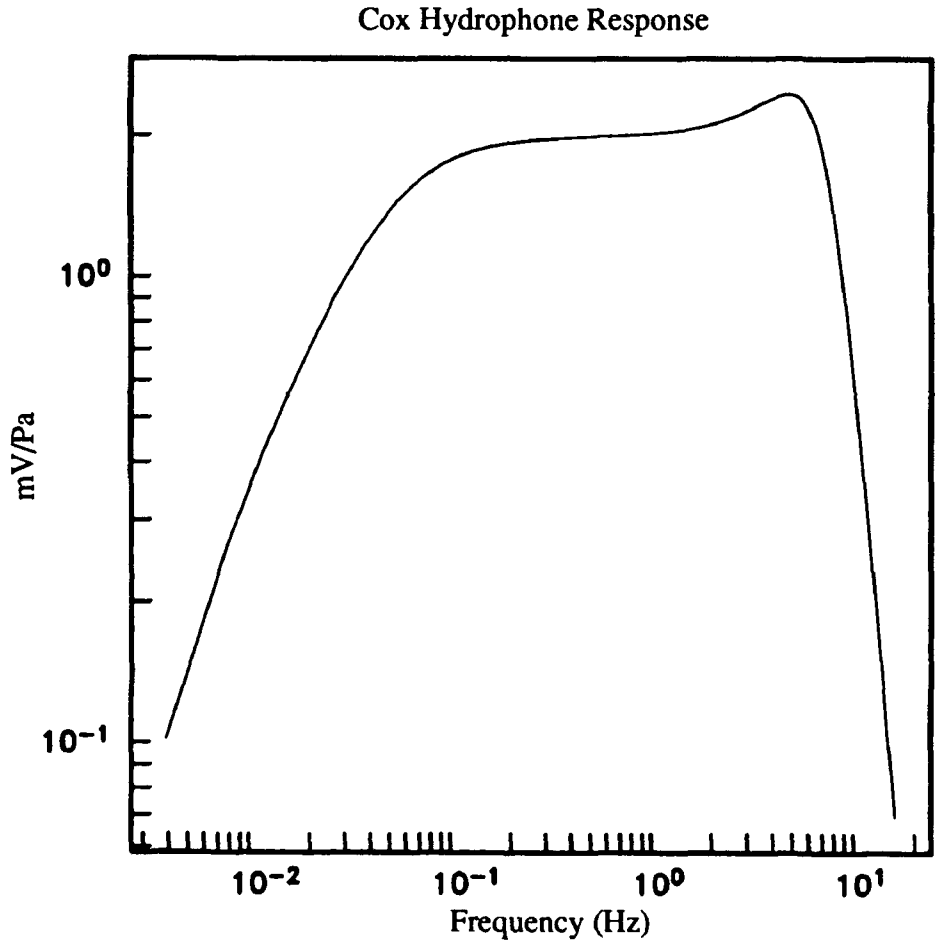

Figure 4: Response function of the OBS hydrophone channel.

km deep water. In the first experiment five OBSs equipped with the Cox hydrophones were deployed for about three weeks, recording simultaneously 17-minute windows every six hours. In the second experiment, in addition to the OBSs, a number of electric field instruments and differential pressure gauges (Webb and Cox, 1986) were deployed as part of the array, all of the instruments carrying a Cox hydrophone. The

instruments were left on the ocean bottom for three weeks. The OBSs were programmed to record 17 minute windows at 4 hour intervals, while the other instruments recorded continuously. The R/P Flip arrived at the site while the last of the instruments were being deployed and drifted above the area for the duration of the

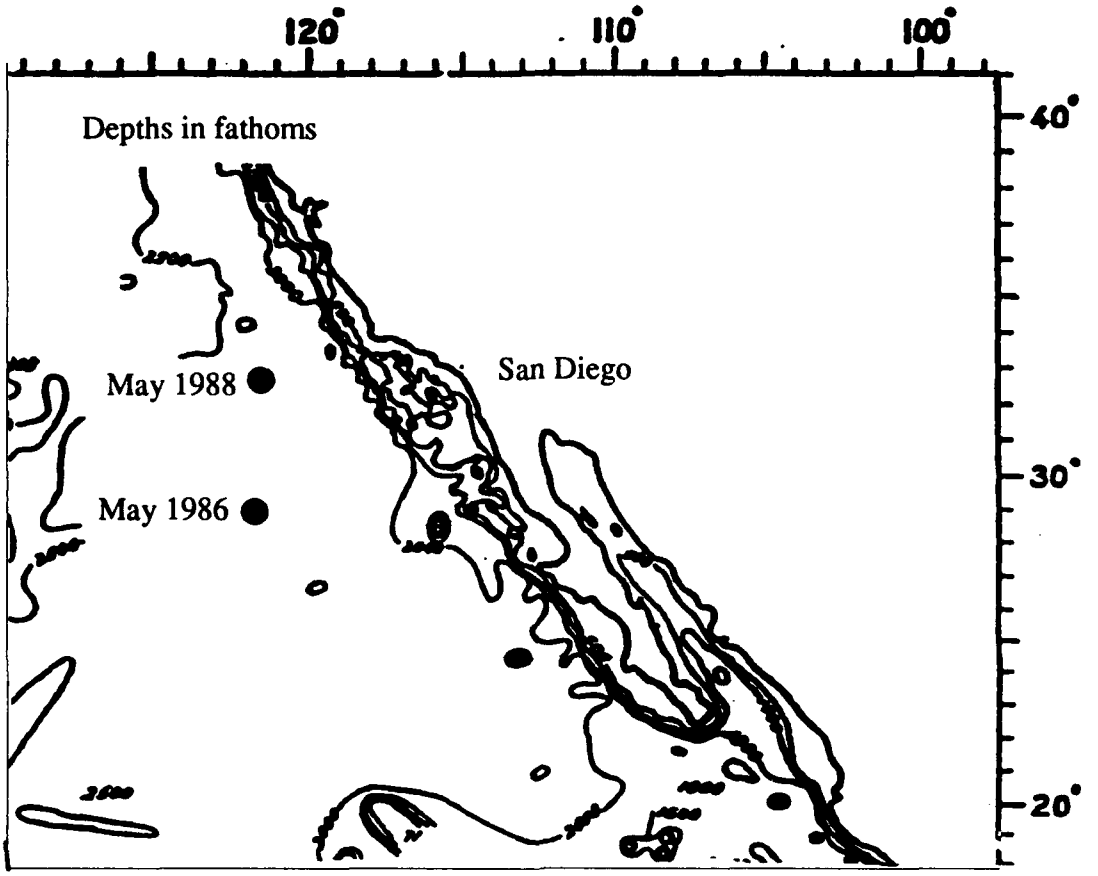

Figure 5: Map of 1986 and 1988 experiment sites.

deployment recording wave spectra and azimuth and local weather conditions. The instruments that contributed data for the analysis are shown in figure 6, but it should be noted, given the dated hardware, that not all instruments provided useful data at the same time, and timing problems prevented using others on certain occasions. The position of the instruments on the ocean bottom, was determined by an acoustic transponder.

Figures 7 a) and b) show the development over time of the pressure spectra for OBS Karen during the 1988 experiment, named the Noise And Coherence Hydrophone and OBS Study (NACHOS). Note the relative stability of the microseism peak, both in amplitude and frequency, throughout the recording period. It is interesting to compare the spectra with the available weather data. The weather data covering the time of the NACHOS deployment came from two sources; local weather was obtained from bridge observations of the R/P Flip which was drifting in the area above the array and weather for the whole Pacific area was

compiled from weather maps of the National Weather Service. Figure 8 shows that the local wind speed between May 12th and May 22nd varied considerably and included periods of stormy weather. Comparison with figure 7 shows a direct dependence of the wide peaks in the frequency band of 0.3-1.0 Hz on the wind intensity. These 'bulges' follow the wind pattern, with a delay of a few hours, suggesting a locally generated phenomenon.

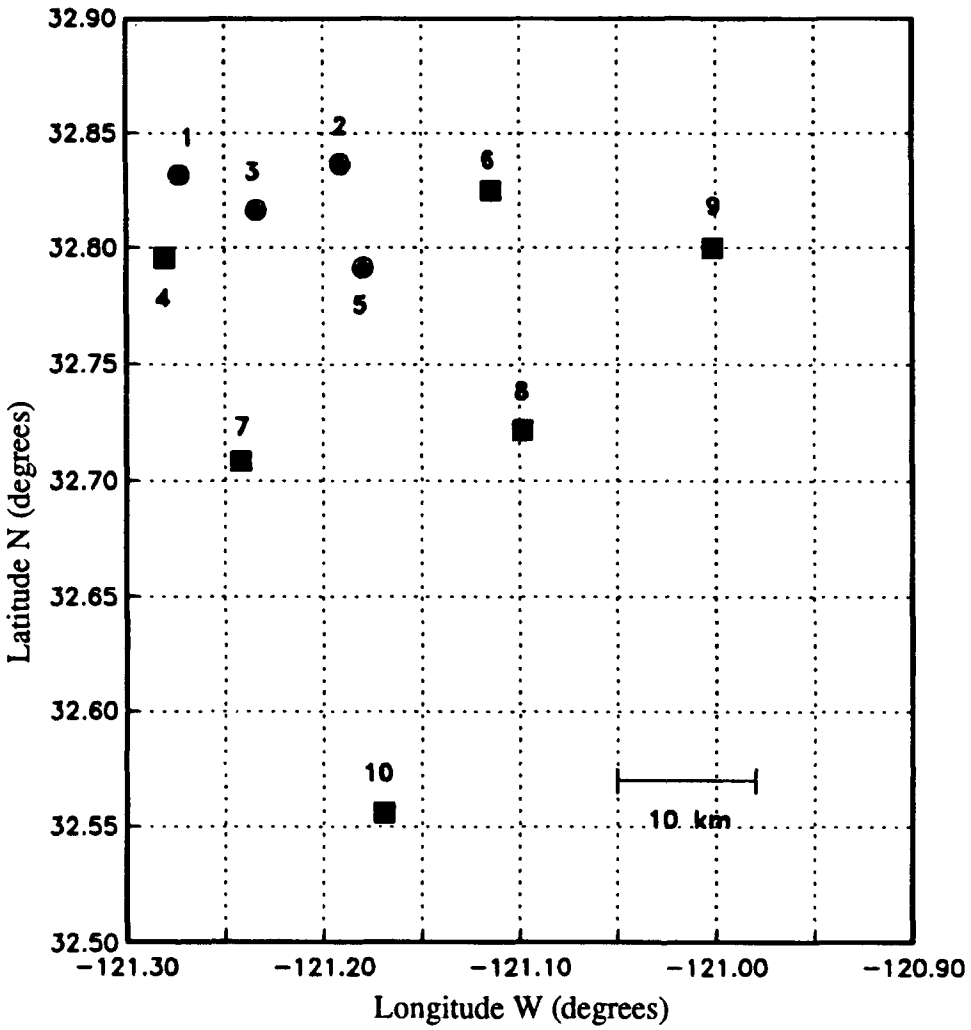

Figure 6: The NACHOS instruments that provided data for the analysis. Circles represent OBSs and squares are pressure gauges.

For the microseism peak around 0.15 Hz, there is no apparent correlation with increases in local wind speed and wave height. It has been suggested that surface gravity waves from large, distant storms are the source of this dominant signal. Surface analysis weather maps of the deployment period show a constant strong low pressure system in the area of the Gulf of Alaska. This storm area is a potential source for microseisms and waves arriving from the Gulf area should display the dispersion relation, $\omega^2 = gk \tanh(kh)$. Assuming deep water waves

$$\tanh(kh) \equiv 1 \quad \text{and} \quad v_{group} = \frac{v_{phase}}{2} = \frac{d}{t - t_0}$$

where d is the distance between source and receiver and t_0 the origin time of the signal, the frequency behaves as $\omega = g(t - t_0) / 2d$ (*Snodgrass et al, 1966*). The distance can then be found from the slope $f/(t - t_0) = g/4\pi d$ where the time t_0 is the point where the line traced through the peaks of the microseisms intersects with $f = 0$. From figure 7 it can be seen that the slope is not well defined and several lines can be traced along

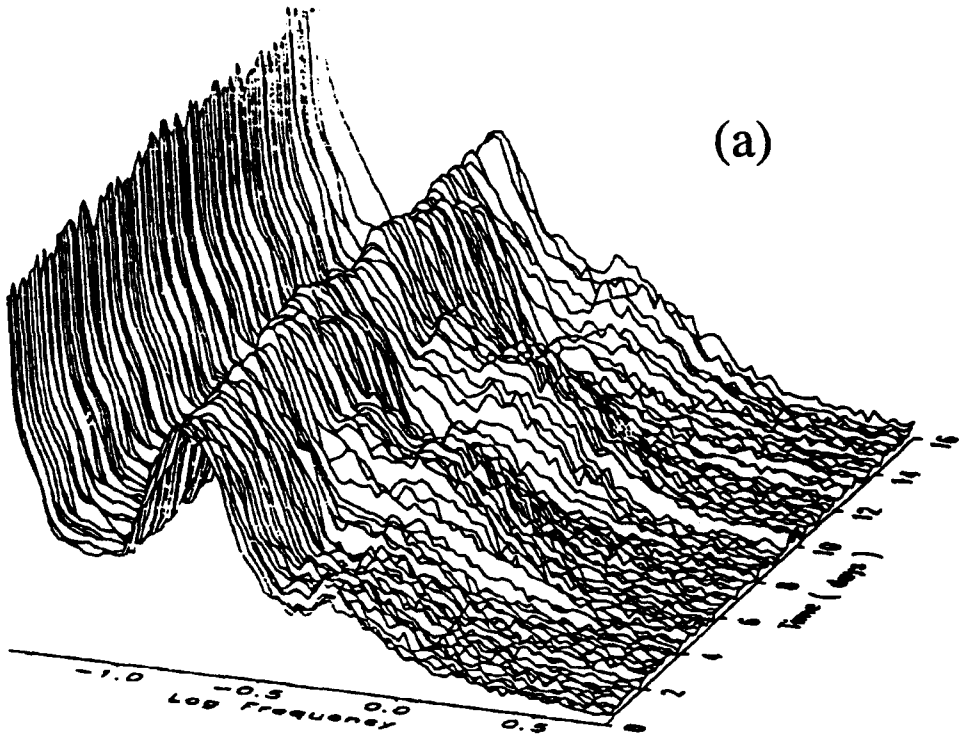

Log Noise Spectrum, Karen Hydrophone

Figure 7: a) Pressure spectra for an OBS hydrophone covering 16 days of the NACHOS Experiment. The 17 minute-long records were taken four hours apart.
b) Same as a) plotted as a contour plot.

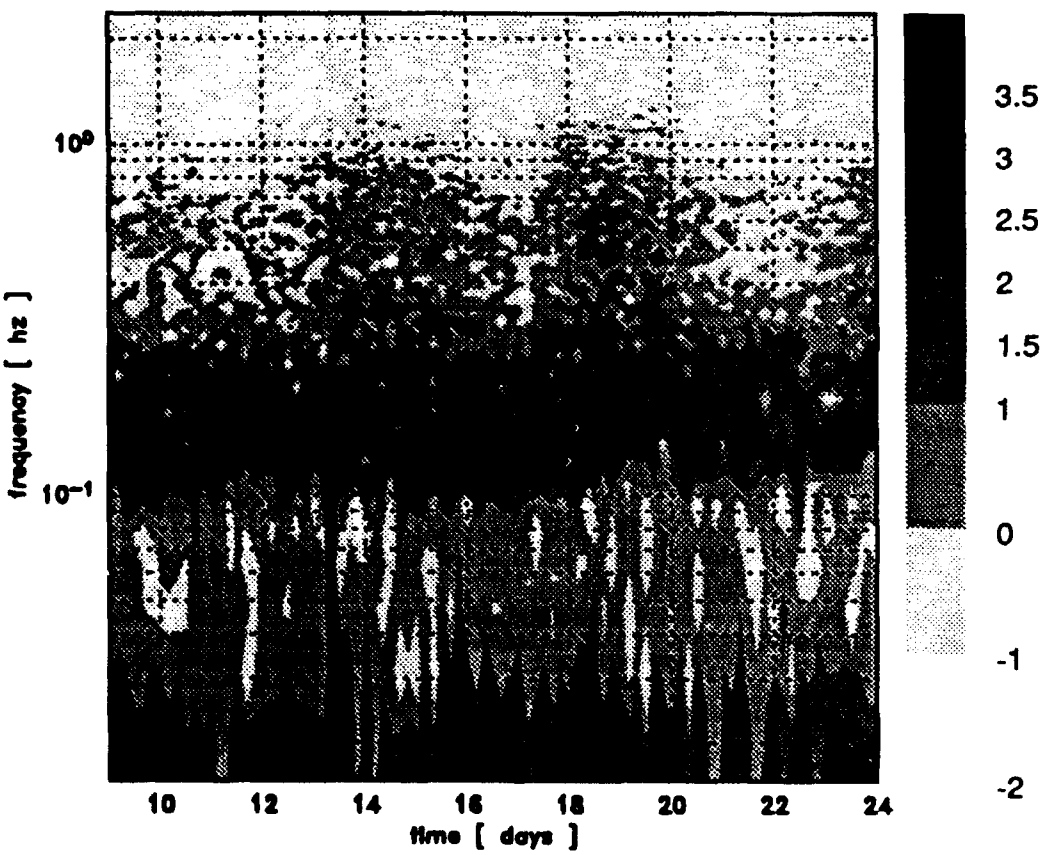

Table 1

Layer	Thickness [km	Vα [km/sec]	Vβ [km/sec]	ρ [kg/m^3]	Qα	Qβ
1	4.1	1.5	0.0	1.0	9999.0	9999.0
2	0.1	1.75	0.2	1.3	100.0	100.0
3	1.9	5.0	2.9	2.8	150.0	300.0
4	6.8	6.8	3.9	3.0	200.0	400.0
5	150.0	7.8	4.3	3.6	200.0	400.0

the microseism peak with different slopes that can be used to infer distances ranging from 2400 km to 6000 km. The distance between the Gulf of Alaska and the experiment site is about 3600 km. Although there appears to be a dispersive trend in the data, it is not clear enough to require a normally-dispersed arrival of the swell responsible for these peaks.

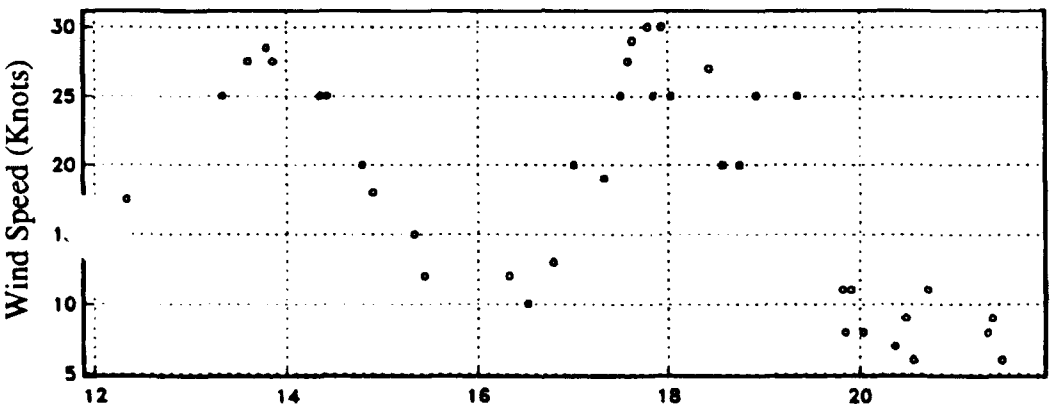

Figure 8: Local wind speed in knots for the NACHOS deployment period, recorded by the R/P FLIP.

The low-frequency peaks

The low frequency end of the microseism peak falls off about 40 dB toward the 'noise notch' which lies in the frequency band of 0.01-0.09 Hz. The spectral level in this band is usually very low, but a peak near 0.08 Hz has been observed on OBSs located close to land (Latham et al, 1967). Based on the 2:1 frequency ratio with the microseism peak and the correlation with the wave spectra on the ocean surface, the peak was explained as the 'single frequency' peak. The existence of the 'single frequency' peak close to the shore might be expected since the wave energy is transferred from the water column to the solid layers at shallow water regions and these waves will be felt at the ocean-bottom interface. However, this low phase velocity signal does not couple readily into propagating elastic waves and so it will decay rapidly away from the coast and will not be felt in the deep ocean.

The 'single frequency' peak was first recorded in the deep ocean by Webb and Cox (1986), but unlike the peak observed near the coast which was continuous in time, the peaks recorded offshore appeared

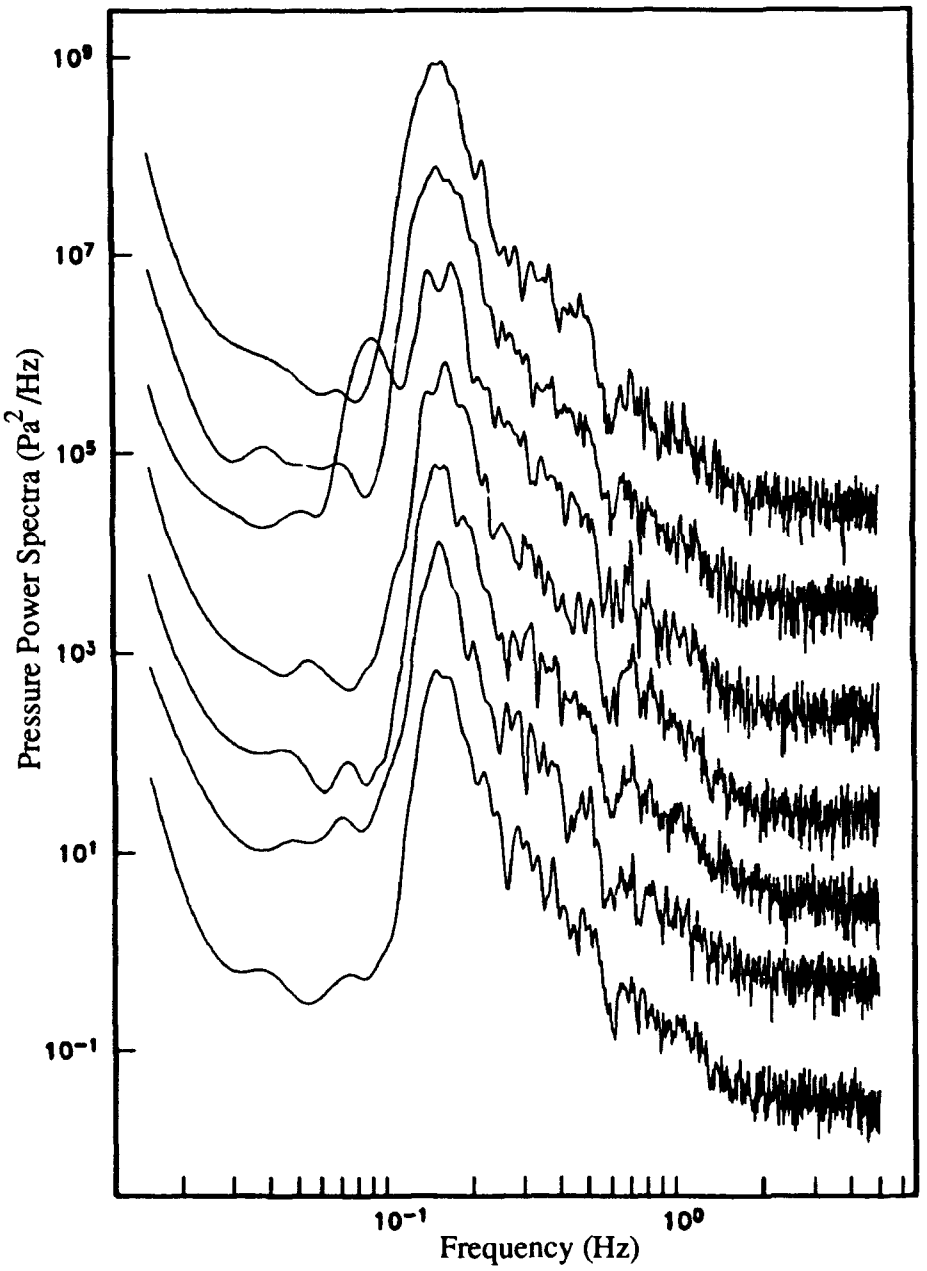

Figure 9: Hydrophone power spectra from 17-minute hydrophone records, recorded 6 hours apart, separated by 10 dB for illustration purposes.

irregularly. Similar peaks, at 0.08 Hz, appeared in the 1986 OBS experiment on four occasions. Figure 9 shows seven consecutive power spectra, which were recorded 6 hours apart, separated by 10 dB for illustration purposes. The fifth spectrum shows the 0.08 Hz peak yet there is no indication that it develops in the preceding spectrum or decays in the spectra following it. In all cases in which the peak appeared, the squared-coherence was exceptionally high, reaching levels higher than 0.9. Plots of coherence-squared and phase from the hydrophone channels of OBSs Phred, Janice and Lynn are shown in figure 10. Seeking a source other than wind waves, a possible explanation arose when event times of earthquakes of magnitude 6 or larger along the Pacific plate boundary were compared with the occurrences of the low frequency peaks. Calculated arrival times for the events of the 1986 experiment show that all the peaks appeared shortly after a major earthquake arrival, although none of the actual arrival times fall inside the 17-minute recording window. A strong earthquake source in the ocean will excite surface waves and the resonant mode known as the 'organ pipe mode' which reverberates in the water column at frequencies of $(n/2 + 1/4)\ v/h$ where $n = 0,1,2,\ldots$, v=1.5 km/s and h is the water depth. In 4.1 km deep water the fundamental mode will have a frequency of 0.09 Hz. Apparently, this signal decays quite slowly over time, since in one event, the signal was still resonating two and a half hours after the calculated arrival time of the earthquake signal.

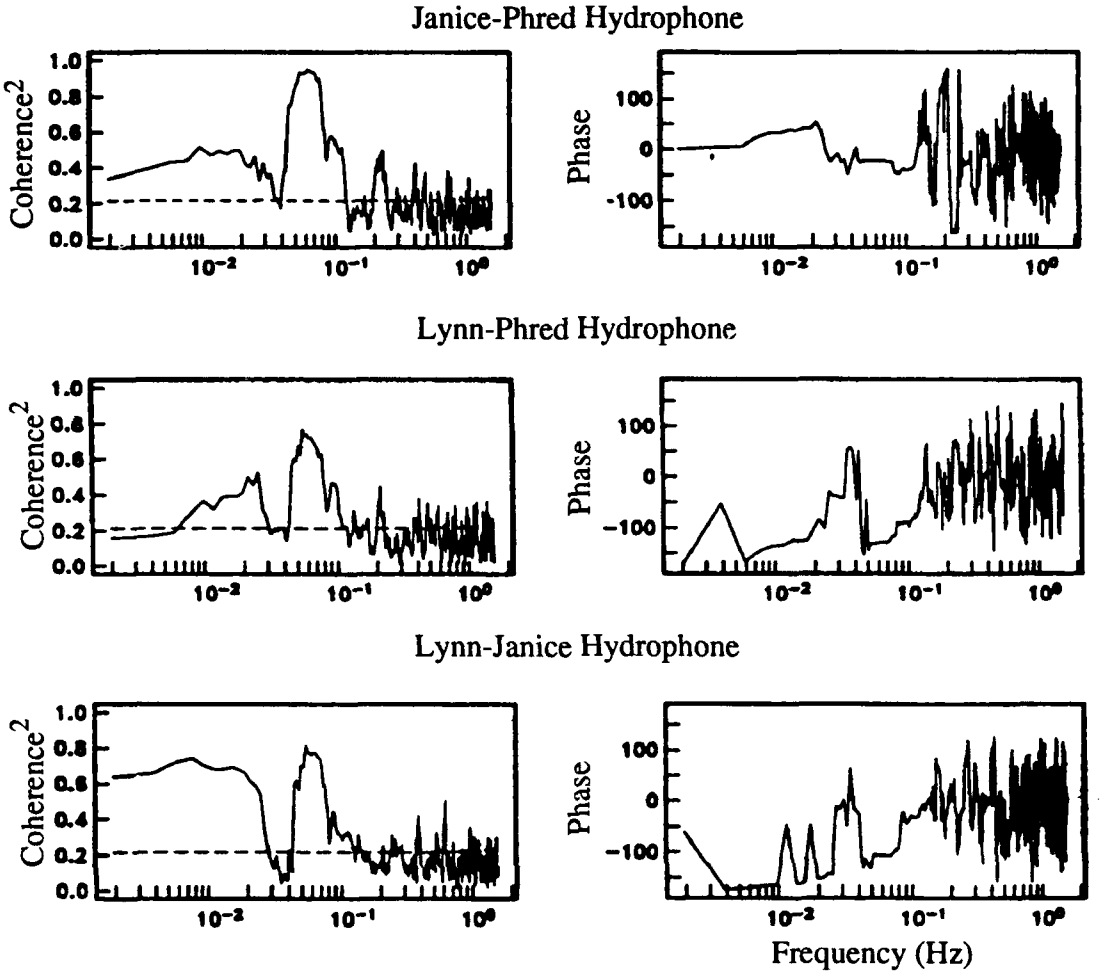

Figure 10: Coherence and phase estimates between OBS hydrophones for the earthquake signal.

In the NACHOS experiment, six pressure gauges that were programmed to record continuously throughout the deployment obtained records of the arrivals of two large earthquake signals. The first earthquake occurred on May 16th 1988 near the Vanuatu Islands in the South Pacific Ocean. It was recorded as a magnitude 6.0 earthquake with a focal depth of 16 km. The second one, on May 17th near the Santa Cruz (Solomon) Islands, registered as a magnitude 6.0 earthquake with a focal depth of 30 km. Figure 11 shows the time series records of the Vanuatu event, from six pressure gauges, filtered with a 0.04 - 0.095 Hz Butterworth filter. The first arrivals are quite clear in all the records and coincide, within the error limits of the model, with those of P-wave arrivals calculated from the Jeffreys-Bullen tables. The signal, which has a period of 11.1 seconds, can be interpreted as the organ-pipe mode reverberations excited by the body wave. The form of the first arrival looks almost identical in all the records and, since there were no calibrating shots fired in this experiment, it was used as a calibrating signal, with the known sensor location and speed of the source. This was necessary due to clock or computer power failures in a few of the instruments at the time of recovery, which did not allow for clock drift corrections. About 23 minutes following the first arrival,

a longer wave train arrives, with a period of about 18 seconds, suggesting surface waves propagating in the shallow lithosphere. These recordings are unique in that the signal propagates along a pure oceanic path from source to receiver, unlike island and coastal stations where the continental shelf or other irregular features scatter and deform the signal close to the receiver. A spectrum of the Santa Cruz earthquake record from pressure gauge no. 7 is shown in figure 12a where two peaks appear in the noise notch - at 0.055 Hz and 0.095 Hz. Figures 12b and 12c are the filtered time series in the frequency bands 0.01-0.07 Hz and 0.07-0.1 Hz

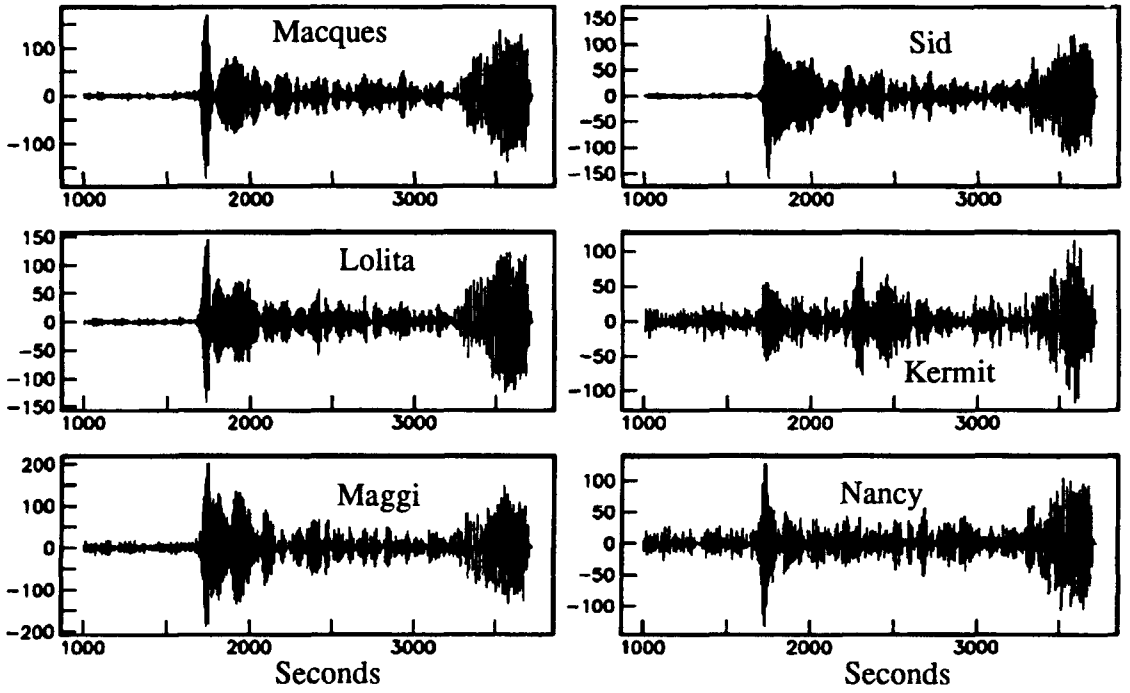

Figure 11: Filtered time series for the Vanuatu earthquake for six pressure gauges. The first arrival and later Rayleigh wavetrain show up clearly.

respectively, showing the signals corresponding to those peaks - the 11 second and 18 second period waves. Speeds calculated from the calibrated arrival times are 3.8 km/s for the surface wavetrain and 9.8 km/s for the body wave. Wavenumber analysis was performed on the earthquake signal using a frequency-domain beamforming technique (Dudgeon, 1977) and a maximum-likelihood filter (Capon et al, 1967). Figure 13 shows the array response in the wavenumber domain for sensors 6-10 (figure 6) which provided the data for the wavenumber analysis. k_x and k_y correspond to the East-West and North-South directions, respectively, and the wavenumber plot describes the response to an impulse signal traveling through the array. Spatial aliasing of the impulse response starts at about 0.05 cyc/km and it is evident from the plot that the resolution in the NE-SW direction is much better than in the NW-SE direction due to the location of the array elements. The frequency-wavenumber analysis plots for two frequencies, 0.0513 Hz and 0.095 Hz, are shown in figure 14. In this representation, a peak in wavenumber amplitude (identical to the array response pattern) indicates the direction from which the signal is coming. The circle around $\mathbf{k} = 0$ represents points of constant velocity

and the line in the WSW direction from the center points to the direction of the earthquake epicenter. As figure 14a shows, the energy at 0.051 Hz propagates with a wavenumber of 0.0122 cyc/km or v = 4.2 km/s from the direction of the earthquake location. As anticipated, the higher frequency signal (figure 14b) propagates at a smaller wavenumber corresponding to a speed of 9.8 km/s, which is the speed used when shifting the first arrival signal for the timing calibration described above. The peak of the body wave arrival is broader than the surface wave peak because the signal-to-noise ratio for the P-wave arrival is lower than for the Rayleigh waves which are propagating largely in the 'noise notch' (see figure 12).

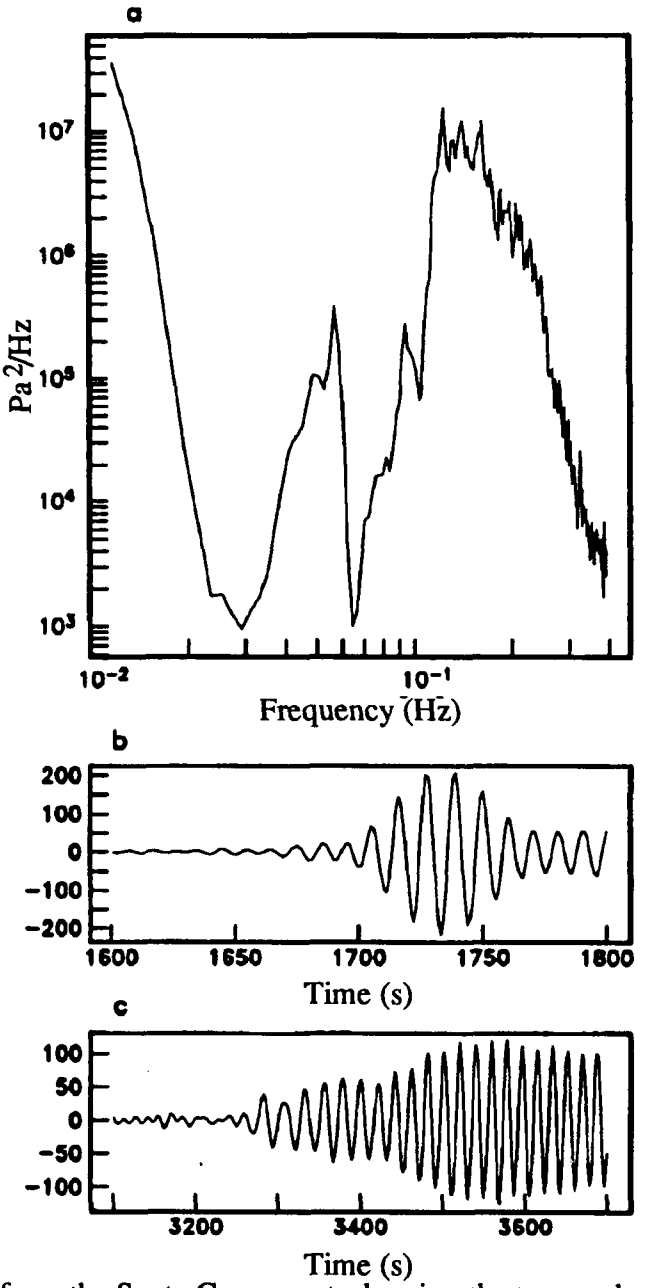

Figure 12: a) Pressure spectra from the Santa Cruz event, showing the two peaks at 0.055 and 0.095 Hz.
b) Filtered time series band passed through 0.07–0.1 Hz showing the arrival of the 0.095 Hz signal.
c) Filtered time series with a band pass of 0.001–0.07 Hz. showing the arrival of the 0.055 Hz wavetrain.

The microseism peak

Unlike the well-defined earthquake signals, the coherence in the microseism band drops significantly. Instruments 1-8 in figure 6 provided the data for the microseism studies. Squared coherence between four pairs of instruments is shown in figure 15 for a period of two weeks. The highest coherence levels appeared between instruments with the smallest separation in the array, 4-5 km. Most marked are the two bands of high coherence, at 0.1 Hz and at 0.2-0.3 Hz; one almost twice the frequency of the other. Note that both coherence bands are not at the microseism peak, the 0.1 Hz band being slightly below the peak frequency and the 0.2-0.3 Hz band somewhat higher than the microseism peak. The phase values for those coherences above the 90% threshold level were plotted for four pairs of sensors at three different frequencies in figure 16. The phase at the microseism frequency appears to be very close to zero and consistent throughout the recording period. The results for sensors 3 and 4 (figure 17) show that most of the points fall within the error bounds at a constant phase of about zero.

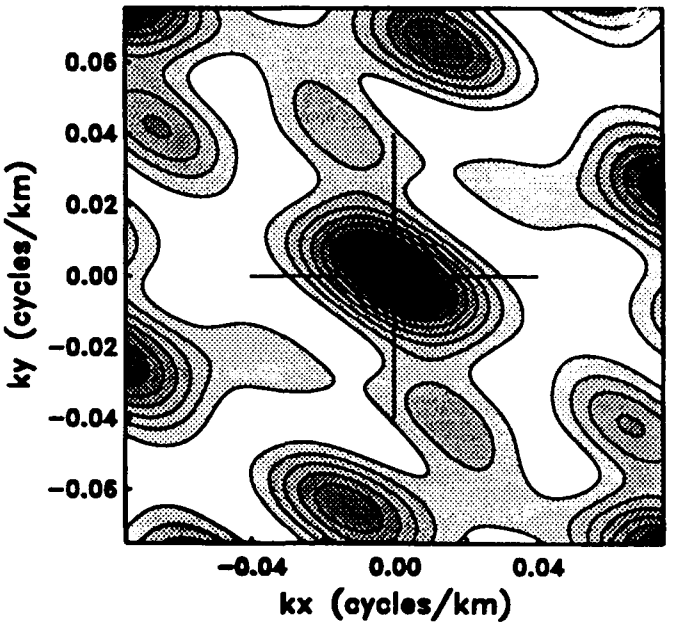

Figure 13: The array wavenumber response for the instruments that provided the data for the earthquake signal beamforming.

This result is similar for all pairs of instruments with separation of less than 6 km (except for the pairs 3,5 and 2,5 where phases appear very scattered). We consider two situations which could result in phase values close to zero for the array. One such case arises when the signal propagates at a phase velocity which is too high for the phase difference to be significantly different from zero. At $f = 0.093$ Hz, the signal has a phase error of $\pm$ 17.5°. The signal would have to travel at a phase velocity of at least 9.6 km/s for the phase difference to be less than 17.5° over a 5 km separation. This is a reasonable result if we assume that the microseisms are traveling as mantle P-waves but is much too high for a Rayleigh wave source. The other situation leading to phase values close to zero occurs when the signal at this frequency is isotropic, in which case the coherence is always real with zero phase (see Webb, 1986). To test this assumption, coherence spectra of an isotropic wavefield were calculated. For a source spectrum $S(\omega,\theta)$ where θ reflects the azimuth, the coherence between a point at the origin and at point (r,ϕ) is

$$\mathrm{Coh} = \frac{\int_{-\pi}^{\pi} S(\omega,\theta)\exp(i\mathbf{k}r\cos(\theta-\Phi))\,d\theta}{\int_{-\pi}^{\pi} S(\omega,\theta)\,d\theta}$$

where k is the wavenumber vector. For an isotropic field, the expression reduces to $Coh(\omega) = J_0(k(\omega)r)$ where J_0 is the zero order Bessel function. This expression was used to calculate coherences for distances ranging from 0.5 to 20 km, where $k = 2\pi f/v$ was determined from the Rayleigh wave phase velocity values calculated for the oceanic model based on Spudich and Orcutt (1980) and shown in table 1. The results, for the fundamental and first mode, are shown in figure 18 where it is apparent that at 0.1 Hz, the coherence is reduced drastically for separations greater than 5 - 6 km. This agrees with the averaged coherence data, incorporated from all the instrument pairs and plotted as a function of separation in figure 19.

The low coherence of the microseism signal supports the assumption of an isotropic source field rather than that of a directional signal. To test the array's ability to resolve directional signals, synthetic spectra for an isotropic field were calculated for the 8-sensor array which was used in the microseism study (sensors

1-8 in figure 6). As mentioned above, the microseism signal was coherent only between instruments separated by less than 10 km, which excludes sensors 7 and 8. Note that the six coherent sensors (sensors 1-6) have a better distribution in the E-W direction than in N-S direction and will, therefore, have an asymmetric wavenumber response. The synthetic modeling of the isotropic wavefield was conducted for the 8-sensor and 6-sensor array for a wavefield propagating at 0.1 Hz and 4 km/sec (figure 20). The difference is quite noticeable; while the larger array detects the signal for 360 degrees, with higher resolution at the NW and SE directions, the smaller array can detect mostly signals coming between W and SW, and E and NE. This is not a very encouraging result, particularly if we assume that microseisms are generated by big storms in the ocean. Signals originating in the area of the Gulf of Alaska would approach the site area from the NNW direction. As for local weather systems, the wind measured on board the R/P Flip shows prevailing north to northwesterly winds. Thus, it seems that with coherence levels rather low in the microseism band, the current data set is not adequate to resolve the spatial characteristics of the signal. Attempts at beamforming, with standard or maximum-likelihood methods, did not produce any consistent results.

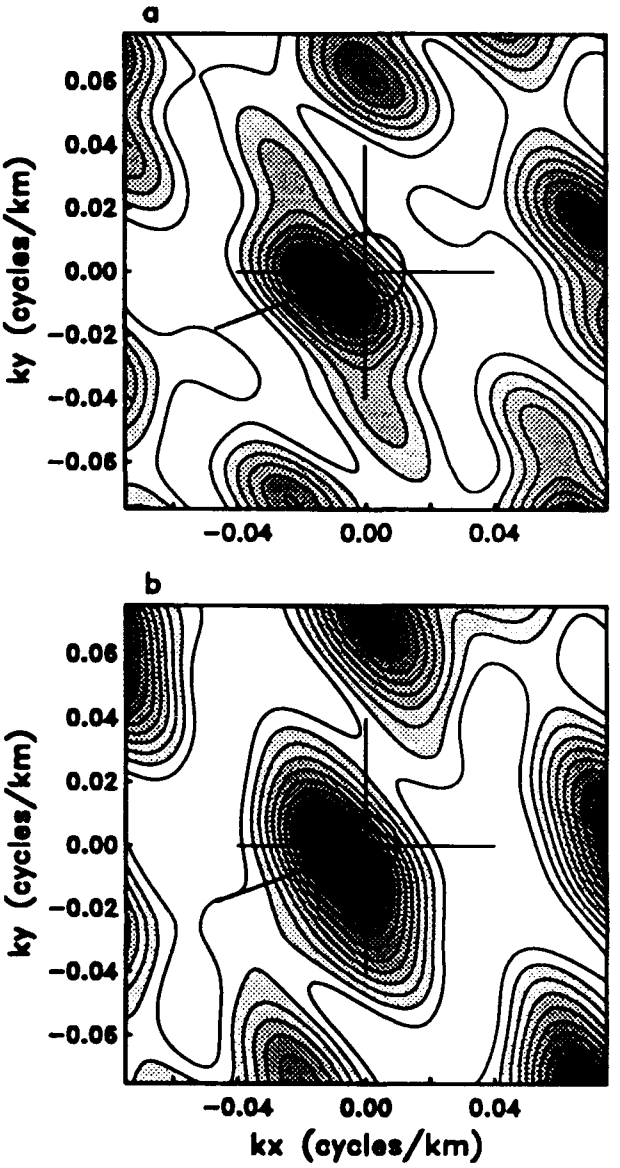

Figure 14: Frequency-wavenumber plots for the Vanuatu event.
(a) for f=0.0513 Hz. The circle represents points of a constant velocity of 4.2 km/s.
(b) f=0.095 Hz and the circle is plotted at v=9.8 km/s. The line indicates the direction to the earthquake epicenter.

Discussion

Recording data on the deep ocean floor offers technical challenges such as the design of instruments that will operate under the special conditions of the sea floor. The data collected in the experiments described in this paper have shown that it is possible to deploy an array of sensors on the deep ocean floor over a period of a few weeks and record coherent signals in the microseism band. Some important points emerge from this study which will certainly be valuable in future seafloor noise studies :

I. The highly coherent peaks in the noise notch that appear for short intervals on seafloor records are earthquake signals - organ-pipe mode reverberations and Rayleigh wavetrains. There was no evidence of the single frequency peak that is observed mostly in ocean bottom records from the Atlantic or in the Pacific

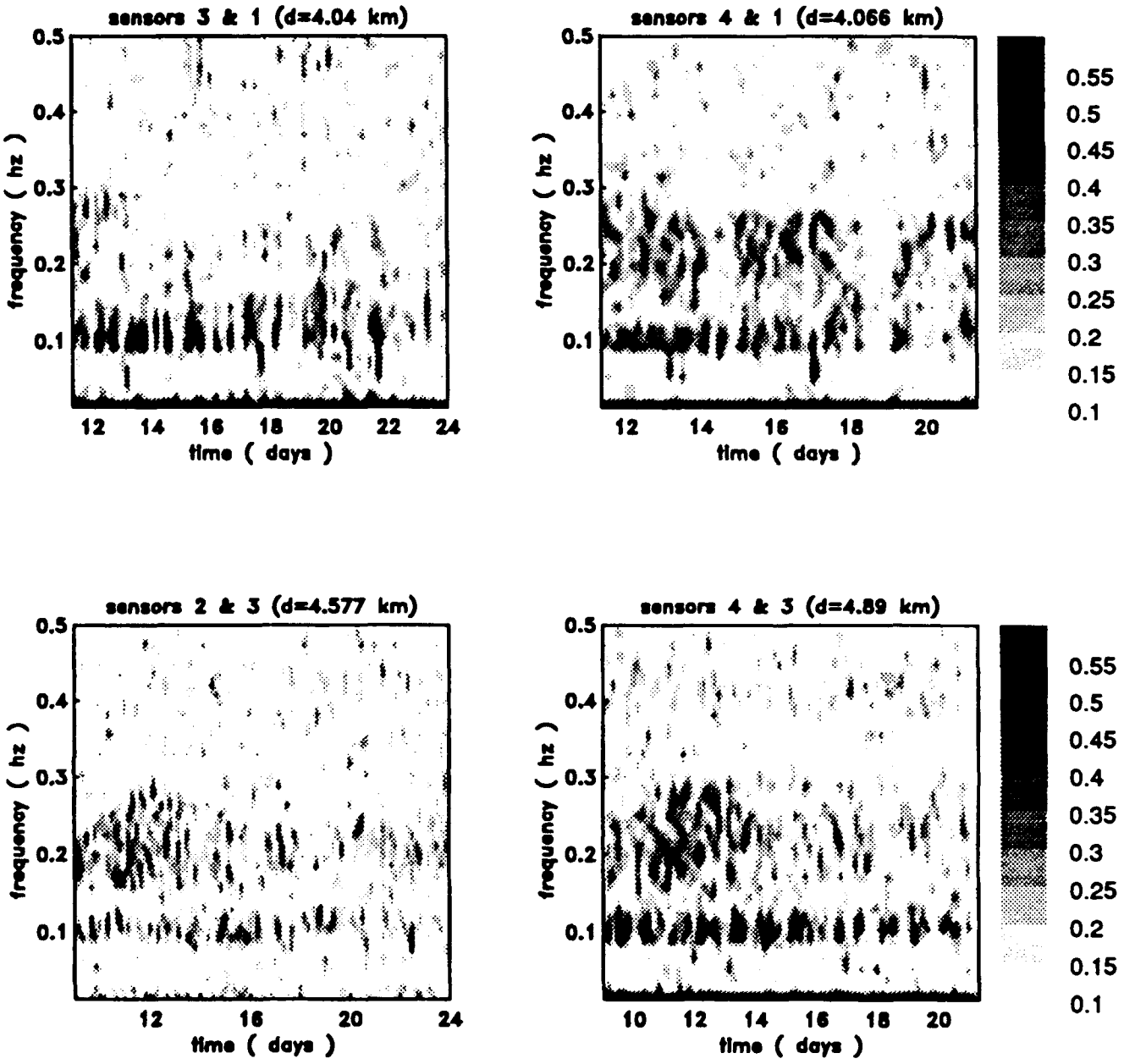

Figure 15: Coherence between four pairs of sensors with the separation in km for 10 days during the NACHOS Experiment. Note the high coherence bands at 0.1 Hz and 0.2–0.3 Hz.

in shallow water.

II. Coherence of the signal in the microseism band is low for sensors separated by distances larger than 6 km. This agrees with results of a recent deep ocean array study in the western Pacific (Webb, 1990). Even when the data were coherent, coherence-squared values rarely reached levels greater than 0.5. It should be noted that the coherent band, around 0.1 Hz, is at the lower frequency edge of the microseism band and that the peak itself is not coherent. It is possible that the higher frequency and shorter wavelength signals are coherent at shorter distances although significant coherence of the peak has been observed at 5 km separation (Cox, personal communication) by using much longer records with more degrees of freedom in the spectra

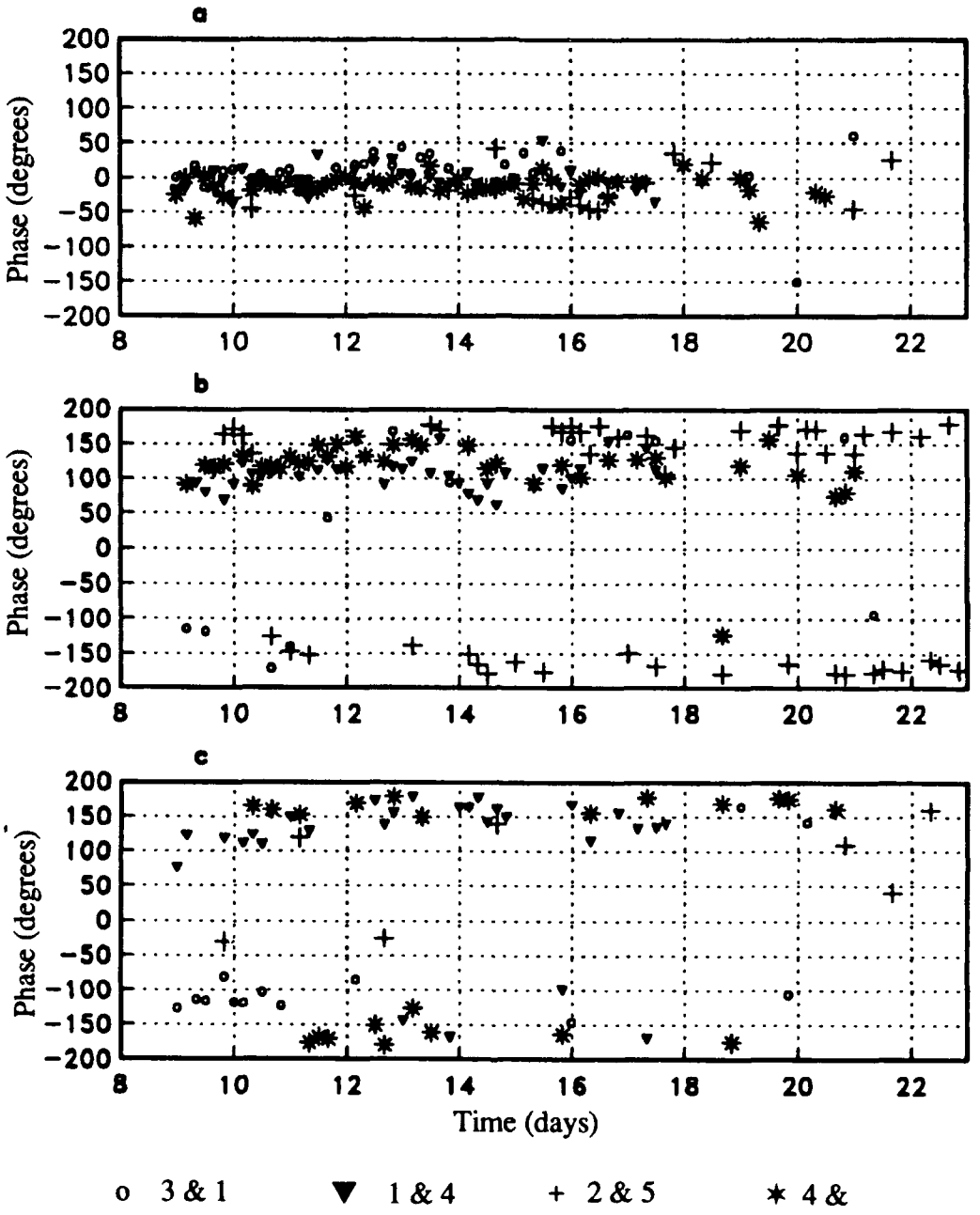

Figure 16: Phase shifts between four pairs of sensors for three different frequencies: a) 0.093 Hz, b) 0.2 Hz, and c) 0.26 Hz.

than available in the data presented here. Another hypothesis is that the microseism signal is locally generated. If most of the signal at the microseism peak was generated by waves backscattered from the coastline (which was 300 miles from the site) and opposing waves, interacting directly above the site, we would expect the coherence to be low. The possibility that part of the signal is short-wavelength Stoneley waves which have a much shorter coherence length (Schreiner and Dorman, 1990) can be ruled out at these frequencies since the dispersion curves for our oceanic model show Stoneley waves only at frequencies higher than 0.3 Hz. From the coherence and phase measurements obtained in this study, it seems that the microseism signal at frequencies close to 0.1 Hz is at least in part isotropic. This is supported by modeling

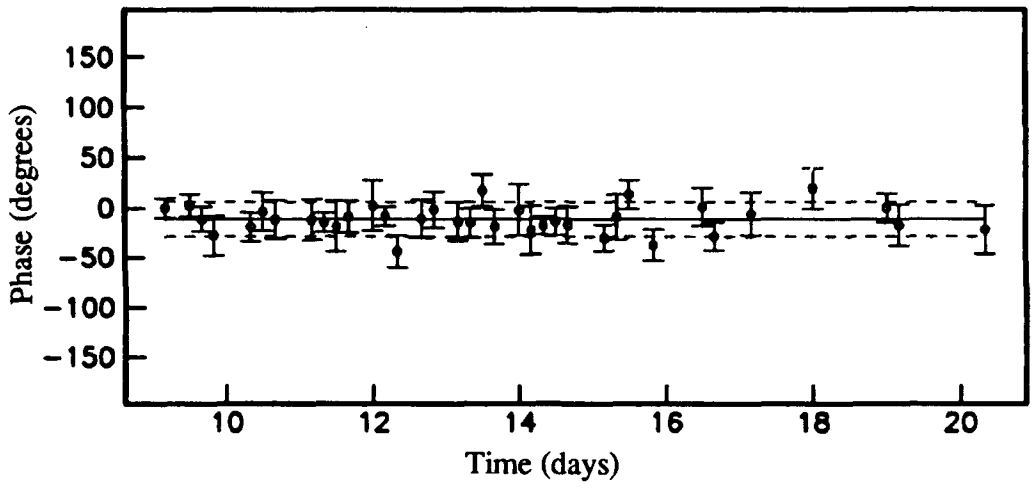

Figure 17: a) The coherence between pressure sensors 3 and 4 during two weeks of the NACHOS Experiment.
b) The phase corresponding to a) with the average phase value (solid line) and average error values (dashed lines).

of an isotropic wavefield with Rayleigh wave characteristics and by the zero phase difference in the coherent signals between pairs of instruments at the microseism frequency. No evidence was found for a directional signal in this band. However, the configuration of the sensors that recorded coherent data in the microseism band is such that a typical microseism signal cannot be detected by the array if it arrives from the NW - the most likely direction for a narrow-beam microseism signal.

III. It was shown that the signals at frequencies between 0.2 and 0.3 Hz were directly influenced by local weather conditions. These signals developed shortly after the local wind increased and disappeared after the wind died. It is interesting that this did not affect the lower frequency microseism peak, and although one would expect the coherence in the microseism signal to improve during periods of good local weather, this is not obvious in the data and the two frequency bands which show high coherence seem to be uncorrelated.

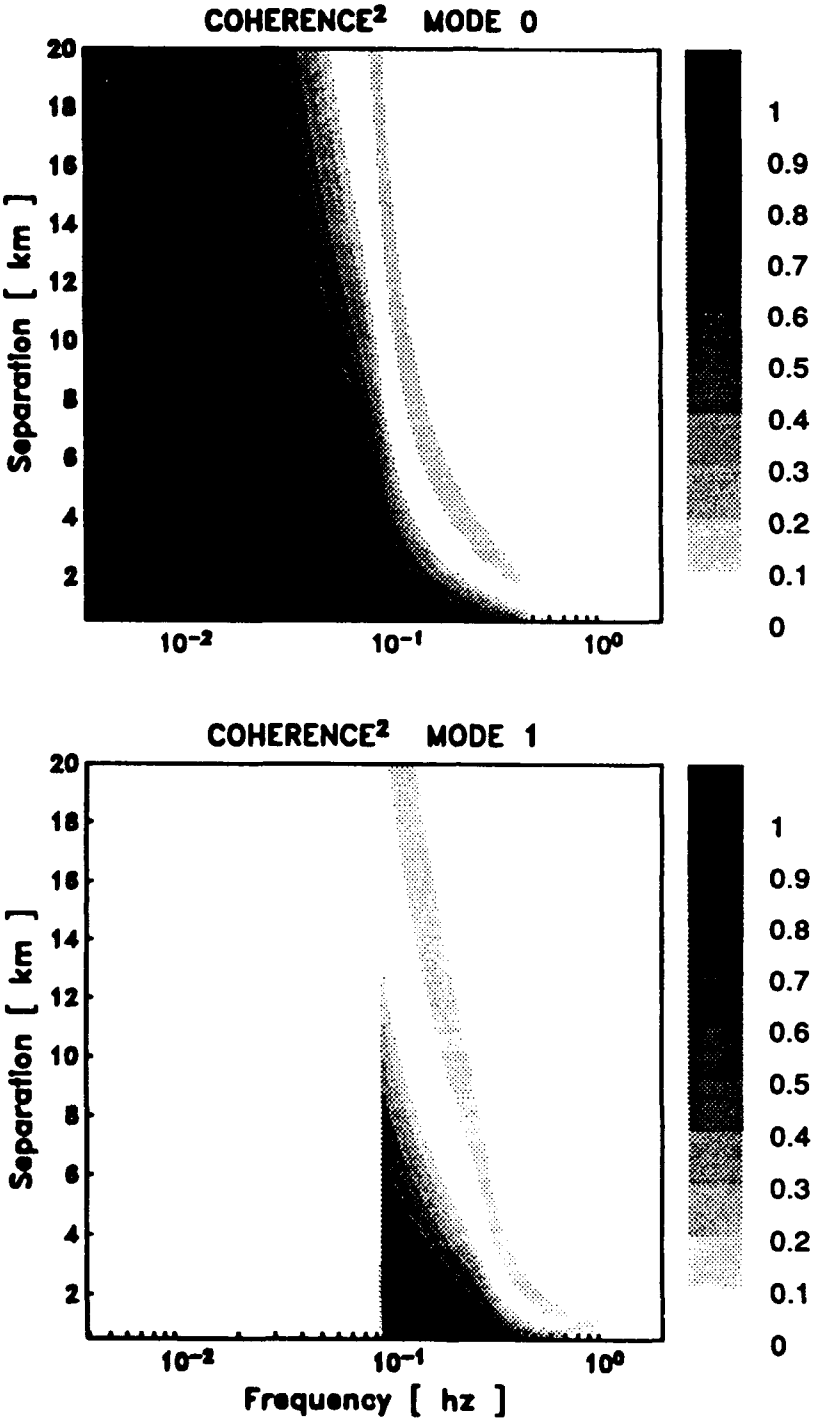

Figure 18: Synthetic coherence model for an isotropic wavefiled for sensors separated 0–10 km apart and using phase velocities calculated from oceanic model I. Upper plot is the fundamental Rayleigh mode and the lower one is the first mode.

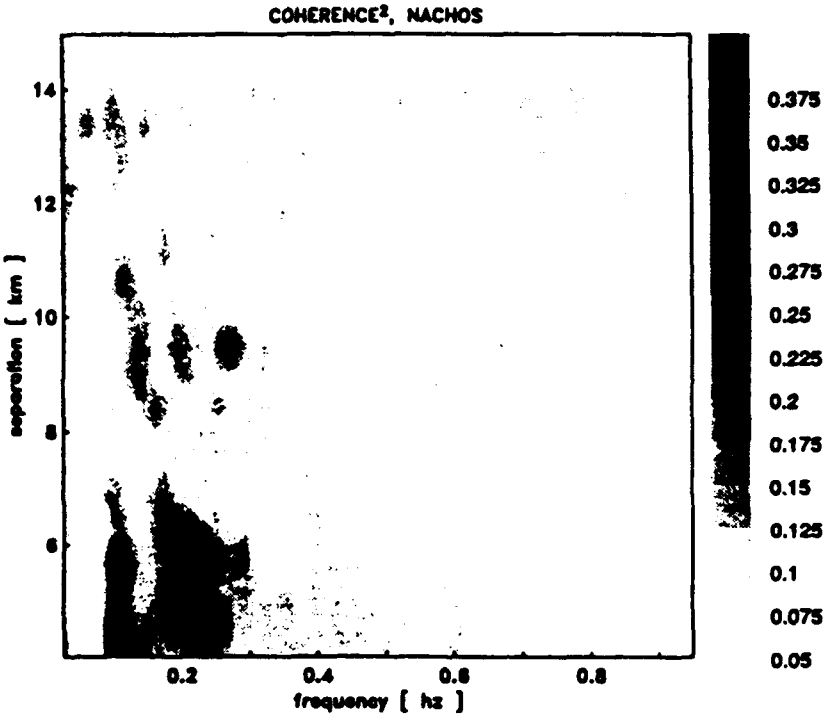

Figure 19: Averaged coherence data from all the NACHOS instruments as a function of separation. Note the drastic decay of coherence for separations greater than 6 km.

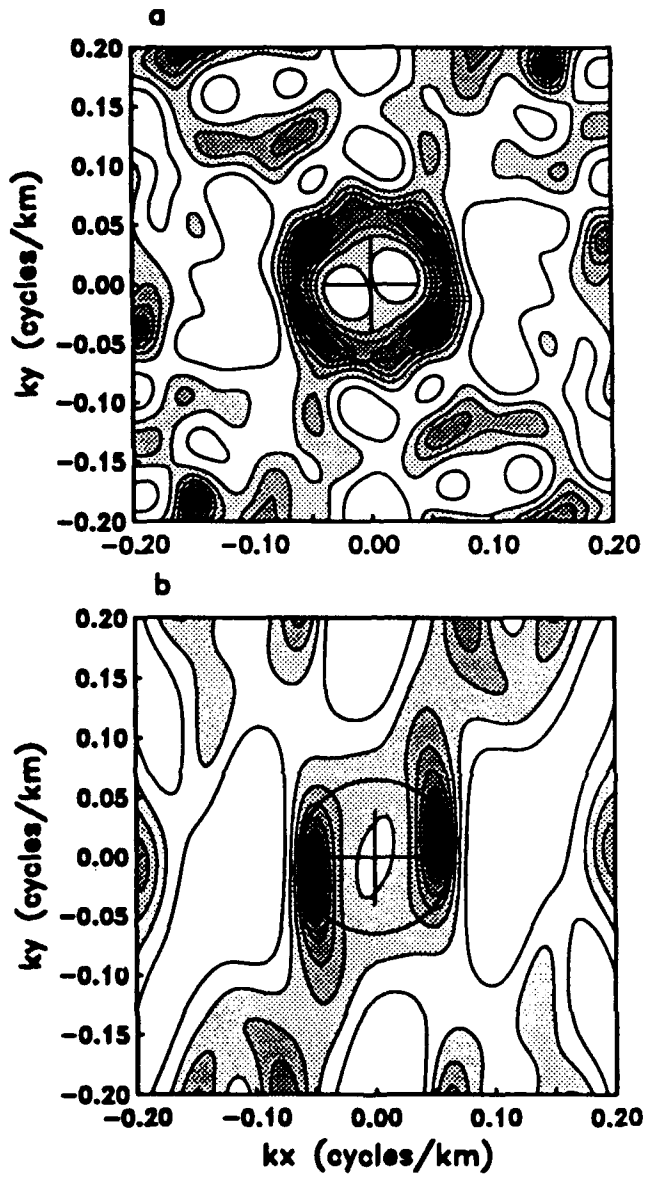

Figure 20: The response of the NACHOS array to a synthetic isotropic wavefield: a) 8-sensor array, b) 6-sensor array.

REFERENCES

Berger, J., D. C. Agnew , R. L. Parker and W. E. Farrell, Seismic system calibration : 2. Cross-spectral calibration using random binary signals. *Bull. Seism. Soc. Am.* **69**, 271-288, 1979.

Capon, J., R. J. Greenfield and R. J. Kolker, Multidimensional maximum-likelihood processing of a large aperture seismic array, *Proc. IEEE*, **55**, 1967.

Cox, C. S., T. Deaton and S. C. Webb, A deep sea differential pressure gauge, *J. Atm. Oceanic Techn.*, **1(3)**, 237-246, 1984.

Darbyshire, J. Identification of microseismic activity with sea waves, *Proc. Roy. Soc. Lon., A.*, **202**, 439-448, 1950.

Dudgeon, D., Fundamentals of digital array processing, *Proc. IEEE*, **65**, 898-904, 1977.

Haubrich, R. A., W. H. Munk and F. E. Snodgrass, Comparative spectra of microseisms and swell, *Bull. Seism. Soc. Am.* **53**, 27-37, 1963.

Kibblewhite, A. C. and K. C. Ewans, Wave-wave interactions, microseisms and infrasonic ambient noise in the ocean, *J. Acoust. Soc. Am.*, **53**, 1032-1039, 1985.

Lahav, D., Observations of low frequency ambient signals in the deep ocean, Master of Sc. thesis, 100 pp., UCSD, 1991.

Latham, G.V., R. S. Anderson and M.Ewing, Pressure variations produced at the ocean bottom by hurricanes, *J. Geophys. Res.*, **72**, 5693-5703, 1967.

Longuet-Higgins, M. S., A theory of the origin of microseisms, *Phil. Trans. Roy. Soc. Lond.*, A, **243**, 1-35, 1950.

Moore, R. D., L. M. Dorman, C. Y. Huang, and D. L. Berliner, An ocean bottom, microprocessor based seismometer, *Mar Geophys. Res.*, **4**, 451-477, 1981.

Orcutt, J. A., C. S. Cox, A. K. Kibblewhite, W. A. Kuperman, and H. Schmidt, Observations and causes of ocean and seafloor noise at ultralow and very-low frequencies, *Proceedings, Natural Physical Sources of Underwater Sound,* in press, 1992.

Orcutt, J. A., R. D. Moore, and T. H. Jordan, Description and performance of the Scripps ocean bottom seismographs during the Ngendei experiment, *Initial Reports of the Deep Sea Drilling Project,* **88/91**, 347-356, 1987.

Nichols, R. H., Infrasonic ambient ocean noise measurements : Eleuthera, *J. Acoust. Soc. Am.*, **69(4)**, 974-981, 1981.

Schreiner, A. E. and L.M. Dorman, Coherence lengths of seafloor noise : Effect of ocean bottom structure, *J. Acoust. Soc. Am., 88 (3)* , 1990.

Snodgrass, F.E., G. W. Groves, K. F. Hasselman, G. R. Miller, W. H. Munk and W. H. Powers, Propagation of ocean swell across the Pacific, *Philos. Trans. Roy. Soc. Lon,* A, **259**, 431-497, 1966.

Spudich, P. K. and J.A. Orcutt, Petrology and porosity of an oceanic crustal site: Results from wave form modeling of seismic refraction data. *J. Geophs. Res.*, **85**, 1409-1433, 1980.

Tyler, G. L., C. C. Teaugue, R. H. Stewart, A. M. Peterson, W. H. Munk and J. W. Joy, Wave directional spectra from synthetic aperture observations of radio scatter, *Deep-Sea Res.*, **21**, 989-1016, 1977.

Webb, S. C. Coherent pressure fluctuations observed at two sites on the deep sea floor, *Geophys. Res. Lett,* **13**, 141-144, 1986.

Webb, S. C. Very low frequency sound studied using multi-element seafloor arrays, *Proceedings, Natural Physical Sources of Underwater Sound,* in press, 1992.

Webb, S. C. and C. S. Cox, Pressure and electric fluctuations on the deep seafloor : background noise for seismic detection. *Geophys. Res. Lett,* **11**, 967-970, 1984.

Webb, S. C. and C. S. Cox, Observations and modeling of seafloor microseisms, *J. Geophys. Res.*, **91**, 7343-7358, 1986.